The Formation of Edge Cracks during Rolling of Metal Sheet

Hermann Riedel[1)], Florence Andrieux[1)], Tom Walde[1,2)] and Kai-Friedrich Karhausen[3)]

[1)] Fraunhofer Institute for Mechanics of Materials, Woehlerstr. 11, D-79108 Freiburg, Germany
[2)] now at Plansee SE, Reutte, Austria
[3)] Hydro Aluminium Deutschland GmbH, Bonn

Many metals tend to develop edge cracks during hot and cold rolling. Edge cracks need to be removed by a trimming operation, and they may cause rupture of the sheet in the rolling mill. Hence, there is a strong motivation to understand the mechanisms of edge crack formation and to develop predictive tools for controlling the phenomenon. The present work explores the applicability of damage mechanics models to this problem. In conjunction with a plausible failure criterion the Gologanu-Leblond model, which is based on non-spherical ductile void growth, is able to predict edge cracking and the characteristic zigzag damage pattern on the edge of the rolled sheet. The experimental determination of the model parameters remains a challenging task, since the stress and strain history at the edge of a rolled sheet is substantially different from the situation in a tensile test, and also from that in other conventional laboratory tests.

Keywords: rolling; process simulation; edge crack; ductile void growth; damage mechanics; finite elements

Introduction

The problem of edge cracking during hot and cold rolling has been observed in steels, silicon iron, aluminum, magnesium, copper and silver alloys [1-3]. The sensitivity of materials to edge cracking generally increases with their strength, and various process parameters, such as the thickness reduction per rolling pass, play a role. Figure 1 shows the appearance of such cracks after heavy cold rolling of an AA5xxx alloy containing 5% Mg. On the side surface of the sheet the cracks form a characteristic zigzag pattern, while in transverse direction they extent a few millimeters from the edge. Before the cracks grow to a critical length in successive rolling passes, they are usually removed by a trimming operation, which, however, causes extra costs and a loss of material. On the other hand, the rupture of the sheet triggered by an edge crack would entail a much greater loss of time and money in the rolling mill or may even cause damage to mill components.

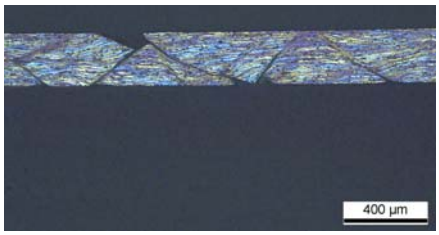

Figure 1. Edge cracks in a cold rolled aluminum sheet viewed in the direction of the roller axis.

The present work is an attempt to improve the understanding of the phenomenon based on the microscopic fracture mechanisms, and to provide a tool for the optimization of materials and processes with respect to edge cracking. Most of the materials that exhibit edge cracking are ductile materials, which fail by void nucleation, growth and coalescence. In aluminum alloys, voids usually nucleate at second phase particles, e.g. at Mg_2Si and $(Fe,Mn)_3SiAl_{12}$ intermetallic phases. Plastic deformation causes the voids to grow and to assume elongated shapes [4]. When the void volume fraction reaches a critical value (typically 3%), the material fractures. The macroscopic fracture appearance resulting from this micro-mechanism depends on the type of test specimen and its possible modes of instability. Examples are the necking and subsequent cup-cone fracture of a round tensile bar, slant fracture of a sheet, and the zigzag pattern of the edge cracks. Figure 2 shows the surface of a crack which started from an edge crack on the right and caused rupture of the strip. Void coalescence leads to a dimpled appearance of the fracture surface. In some of the dimples, the void-nucleating particles are still visible.

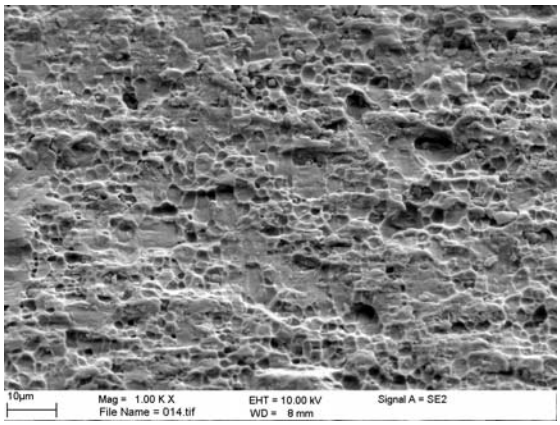

Figure 2. Ductile fracture surface of a ruptured Al strip. Crack starts as an edge crack from the right.

The Gurson [5] model is the classical damage mechanics model for plastic materials containing voids. It is based on the analysis of the plastic deformation fields around spherical voids. The resulting plasticity law depends on the void volume fraction f (also called porosity), which grows or decreases depending on the stress state. Limitations of the Gurson model were discussed extensively in the literature [6-9] in relation to both, experiments and numerical cell model calculations. Most of the limitations arise from the facts (1) that only spherical voids are considered and (2) that the model is generally too stable, i.e. it does not describe strain localization to a narrow sheet of voids properly. In fact, an attempt to model edge cracking with the Gurson model was not successful in the present study. The model predicts diffuse damage at the bulging edge of the sheet with no tendency, however, to localization into the zigzag pattern shown in Figure 1.

Therefore in the present work the porous-plasticity model of Gologanu et al. [10,11] is used, which is a generalization of the Gurson model to spheroidal void shapes. The two models share the drawback to be unable to predict strain localization properly. However, in combination with fracture criteria taking the void shape into account, the Gologanu model is able to describe edge cracking, which is shown in the present paper.

Previous authors have usually modeled cracking during forming processes in a simpler way. Instead of using a damage mechanics model, like the Gurson or Gologanu model, in which stress and damage are fully coupled, most authors employ a conventional incompressible plasticity law to calculate stress and strain and delete elements in which a prescribed phenomenological fracture criterion is fulfilled. A great number of such criteria have been proposed, some being based on critical strain, others on critical stress, others on plastic work. Most of them consider the stress triaxiality, and a few consider the straining history. Among the most popular ones are the strain-based forming limit diagram for predicting cracks in deep drawing, the Johnson-Cook model [12] and the history-dependent criterion of Hooputra et al. [13]. Wierzbicki et al. [14] compare seven of these phenomenological criteria with experiments on an aluminum alloy. They find that three or four of the criteria are consistent with the particular set of experiments on which the study was based.

It is well possible that one or the other of these criteria is able to describe edge cracking, if the model parameters are appropriately chosen. In fact, the present team has already demonstrated in a previous study [15] that the Johnson-Cook model can reproduce edge cracks, though with unreasonable model parameters. In the present paper, at any rate, we prefer to employ the Gologanu model, although it is much more complicated than the mentioned fracture criteria. On the other hand, since it is related to a specific failure mechanism in a well-defined way, it is likely to cover a wide range of stress states, and it allows tracing the evolution of internal damage variables over the processing history, which is important for modeling many consecutive rolling passes.

Although this paper focuses on modeling aspects and on the demonstration of feasibility, it also presents some experimental results and explores the question which type of test is suitable for determining the model parameters that are relevant for edge cracking.

The Damage Mechanics Model

Gologanu-Leblond model. The model of Gologanu et al. [10,11] is an extension of the Gurson model. While the Gurson model describes the growth of spherical voids by plastic flow and the influence of these voids on the plastic properties of the material, the Gologanu model considers spheroidal voids (i.e. ellipsoids with rotational symmetry). Thus the model contains two internal variables, the porosity f (= void volume fraction) and the void shape factor $S = \ln(a/b)$ (a, b = semi-axes of the ellipsoid). Like the Gurson model, the Gologanu model is

formulated in terms of a flow potential Φ, which depends on the stress tensor and on the internal variables, and which defines the yield condition, Φ = 0, and the flow rule, $\dot{\varepsilon}_{ij} \propto \partial\Phi / \partial\sigma_{ij}$. The flow potential also contains the hardening curve of the (void-free) matrix material, σ_M, and a (meaningless) adjustable parameter q_1, which is chosen as $q_1 = 1.5$.

Further, the Gurson and the Gologanu models include an equation for the rate of void nucleation

$$\dot{f}_{nuc} = \frac{f_N}{\sqrt{2\pi}s_N} \exp\left(-\frac{1}{2}\left(\frac{\varepsilon_e^{pl} - \varepsilon_N}{s_N} \right)^2 \right) \dot{\varepsilon}_e^{pl} \qquad (1)$$

where ε_e^{pl} is the equivalent plastic strain, and f_N, s_N and ε_N are parameters having the following meaning: f_N is the total void volume fraction that can be generated by nucleation alone, ε_N is the strain at which the nucleation rate has a maximum, and s_N is the width of the distribution function of strains over which voids nucleate. In the present paper, the nucleation rate is set to zero if the hydrostatic stress is less than 100 MPa, since it is plausible that no or fewer voids nucleate under compressive or small tensile stresses.

The Gologanu model has one preferred direction, namely the axis of rotation of the ellipsoids, while the other two directions are equivalent. This does not quite correspond to the situation in a rolled sheet, where all three directions are different. Hence, it is necessary to decide which of the three directions in the sheet should be the preferred direction of the model. The most plausible choice for the preferred direction is the rolling direction. The model does not include evolution equations for the void orientation (see the Discussion).

Fracture criteria. Both the Gurson and the Gologanu models predict final fracture in principle, but the prediction is reasonably accurate only for high stress triaxialities, while for low triaxiality, both models are too stable and in fact do not predict fracture at all, for example for uniaxial tension. Hence, it is necessary to impose fracture criteria.

In this paper, a combination of two criteria is used; fracture occurs once the first of the two is fulfilled. In Fig. 3, the geometrical quantities are defined which are used in the criteria.

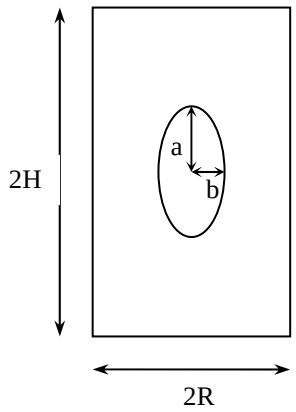

Figure 3. Geometry on which the fracture criteria are based. Spheroid with semi-axes a and b, dimensions of the unit cell H and R

Among the two criteria the Thomason criterion [16,17] usually dominates at high triaxiality. Its form is

$$C_{\text{Thomason}} = \frac{2\sigma_e}{3\sigma_M} + \frac{|\sigma_m|}{\sigma_M} - A\, C_f = 0 \qquad (2)$$

with the von Mises equivalent stress σ_e, the hydrostatic stress σ_m, the matrix flow stress σ_M, and

$$A = 1 - (b/R)^2 \qquad (3)$$

$$C_f = \alpha\left(\frac{R-b}{a} \right)^2 + \beta\left(\frac{R}{b} \right)^{1/2} \qquad (4)$$

with $\alpha = 0.1$ and $\beta = 1.2$ according to Pardoen and Hutchinson [17]. The ratio b/R varies with the deviatoric strain component in the preferred direction, ε'_{22}, according to

$$\frac{b}{R} = \left[\frac{3}{2} \frac{bf}{a} \frac{H_0}{R_0} \exp\left(\tfrac{3}{2} \varepsilon'_{22}\right) \right]^{1/3} \tag{5}$$

where the subscript 0 denotes the initial value, while the ratio a/b (= exp S) and the porosity f are calculated by the Gologanu model.

At low triaxialities the Brown and Embury criterion dominates [18]. It contains only geometrical quantities in the form

$$C_{Embury} = \sqrt{a^2 + b^2} - R = 0 \tag{6}$$

The ratio a/b is taken from the Gologanu model, and b/R is

$$\frac{b}{R} = \left[\frac{bf}{a} \frac{H_0}{R_0} \exp\left(\tfrac{3}{2} \varepsilon'_{22}\right) \right]^{1/3} \tag{7}$$

In the simulation of rolling, usually the Brown-Embury criterion becomes critical first, while the tensile test is terminated by the Thomason criterion. The rationale behind the Thomason criterion is that fracture occurs once the ligament between voids becomes unstable against tensile collapse, whereas the Brown-Embury criterion is derived from the argument that failure occurs once the ligament between neighboring voids can accommodate a 45° shear band. Especially the Brown-Embury argument is admittedly crude and future work should aim at better criteria. Multi-void models as those shown in the Discussion could serve as a basis for such an improvement.

The Gologanu model together with the combined Thomason and Brown-Embury criteria was implemented as a user defined material model (VUMAT) in the finite element program ABAQUS/Explicit.

Experiments and Parameter Adjustment

Sheets of an AA5xxx alloy were supplied by Hydro Aluminium in cold rolled condition with 1.2 mm thickness. This alloy is particularly sensitive to edge cracking when deformed to high strains. Tensile specimens according to Figure 4 were cut from the sheets in rolling, transverse and 45° direction. The strain rate during the tensile tests was 10^{-3}/s.

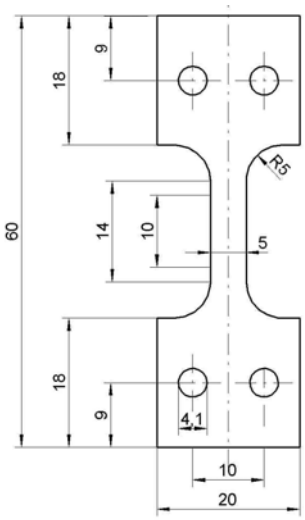

Figure 4. Tensile test specimen

The tests were modeled with the damage model described in the previous section in order to determine the hardening curve of the matrix material, $\sigma_M(\varepsilon)$, the parameters of the Gologanu model, f_N, ε_N and s_N, and the

initial values of the porosity, f_0, of the shape factor, S_0, and of H_0/R_0. The hardening curve of the matrix material was considered isotropic, i.e. the influence of crystallographic texture was neglected. Whereas the hardening behavior was in fact nearly isotropic, the strain to fracture depended markedly on the test direction with the rolling direction having the smallest ductility (about 9% strain to fracture). The Gologanu model can describe the anisotropic ductility, since the initial voids have already elongated shapes from previous rolling passes, and this leads to lower ductility in rolling direction.

This paper presents the adjustment of the model only to the tensile tests in rolling direction (Figure 5). As the figure shows, the material exhibits pronounced oscillations of the stress which are probably due to dynamic strain ageing (the Portevin-LeChatelier effect), which is not included in the present model. Otherwise, the fit to the experimental data is good.

Für Herausgeber: Vorsicht: das Textfeld 'model' mit dem Pfeil ist nicht mit der Grafik verbunden

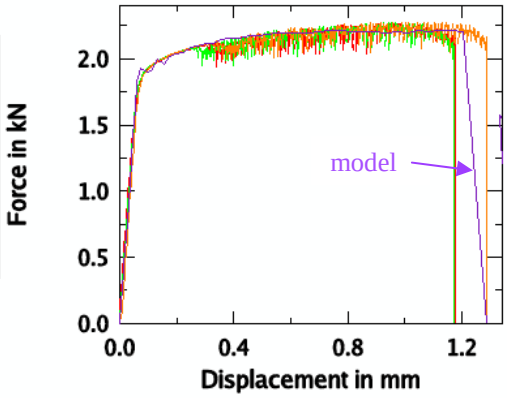

Figure 5. Measured and adjusted force-displacement curves for tensile tests in rolling direction. The model does not describe the oscillations due to dynamic strain ageing.

Figure 6 shows an example for the stress distribution in the specimen in the plastic state before fracture (left). Only one eighth of the specimen is modeled because of the symmetry of the problem. The right picture shows part of the gauge length, where fracture has occurred at a higher load. The failed elements, displayed in blue, form a damage pattern containing a region where the fracture surface is normal to the applied stress, and a shear fracture zone near the edge. The pattern obtained in this three-dimensional simulation resembles that obtained with a multi-void model for plane strain tension (Figure 16 below).

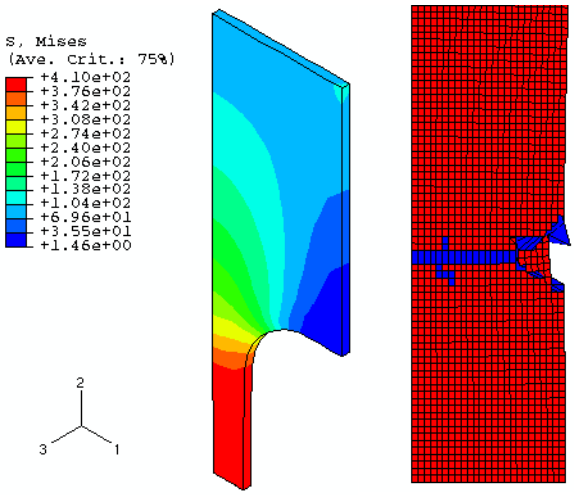

Figure 6: Stress in the tensile specimen before fracture (left). Fracture in the gauge length with failed elements in blue (right).

The adjustment of the damage model to the tensile tests allows determining the model parameters with some confidence, except the initial porosity f_0 (see the Discussion). A numerical value $f_0 = 0.0016$ is chosen, but also other values would be consistent with the tensile tests.

Rolling Simulation

Technological parameters. The initial sheet thickness 1.2 mm is reduced in two cold rolling passes to thicknesses between 0.5 and 0.55 mm. The technological parameters (reduction in each pass, work roll diameters, speed, uncoiling and coiling stress) are chosen according to the conditions in an industrial rolling mill, and variants are investigated with respect to their influence on edge cracking.

The finite element model. Only a quarter of the sheet is modeled as a cuboid with dimensions 92 x 50 x 0.6 mm in rolling, transverse and thickness direction. The assumption of symmetry in thickness direction is not ideal, since the zigzag pattern of the edge cracks may or may not be symmetric, but for the present purpose to demonstrate feasibility, the assumption is acceptable. Figure 7 shows the mesh refinement near the edge of the sheet, where the initial element size is 0.2 x 0.2 x 0.1 mm. The number of elements is 55,200, and there are 203,300 degrees of freedom. With the mass scaling used in the calculations the first pass requires about 60,000 time increments, and the second about twice as many (because of the smaller element size after the first pass). Typical computing times for two passes are 22 h on a 64 bit SGI Altix workstation. So far, no efforts were made to optimize computing times.

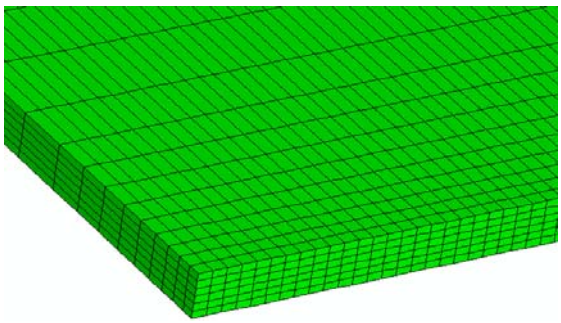

Figure 7. Finite element model with mesh refinement near the edge of the sheet. The rolling direction is horizontal.

Results. A previous study [15] with assumed material parameters has already demonstrated that the damage model proposed here can predict edge cracks in principle. Figure 8 shows the characteristic zigzag pattern for a simulation with symmetry conditions in thickness direction. The simulated pattern is remarkably similar to the observed one (Fig. 1).

Figure 8. Zigzag pattern connected with edge cracking (from [15]). The elements with marked boundaries have failed.

Other than the previous demonstration example, the following results are valid for the actual material parameters of the AA5xxx alloy. The sequence of Figures 9 to 11 refers to the first pass. The sheet moves from left to right. The edge of the sheet is on the top of the picture, the centerline is at the bottom. The roll gap is identifiable by the color contrast.

Figure 9 shows the compressive stresses in the roll gap, which exceed 900 MPa near the center, and are much smaller near the edge of the sheet (about 300 MPa).

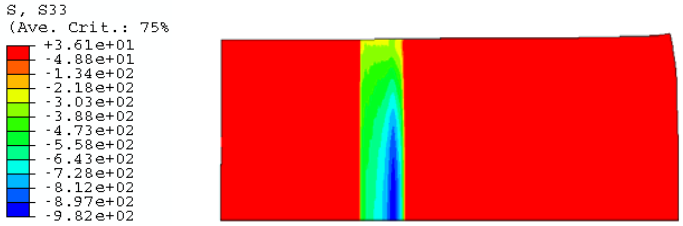

Figure 9. Stress in thickness direction during first pass.

Figure 10 demonstrates that there are tensile stresses in rolling direction greater than 300 MPa near the edge of the sheet directly after the roll gap, while the residual stresses further away are about 130 MPa. No edge cracks appear in the first pass, but the relatively high tensile stresses near the edge induce incipient damage, which leads to crack formation in the second pass.

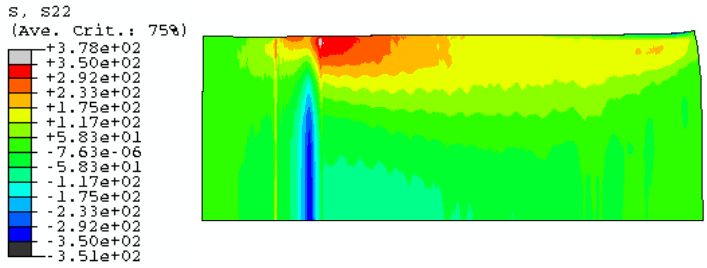

Figure 10. Stress in rolling direction during first pass.

Figure 11 shows the void volume fraction f, and the void shape factor S. The initial values are $f_0 = 0.0016$ and $S_0 = 0.6$. As one would expect rolling reduces the porosity, but f increases slightly and temporarily directly after entering the roll gap near the edge of the sheet. The voids grow elongated during rolling, i.e. S increases to values around 2.5 in the centre and 1.7 near the edge.

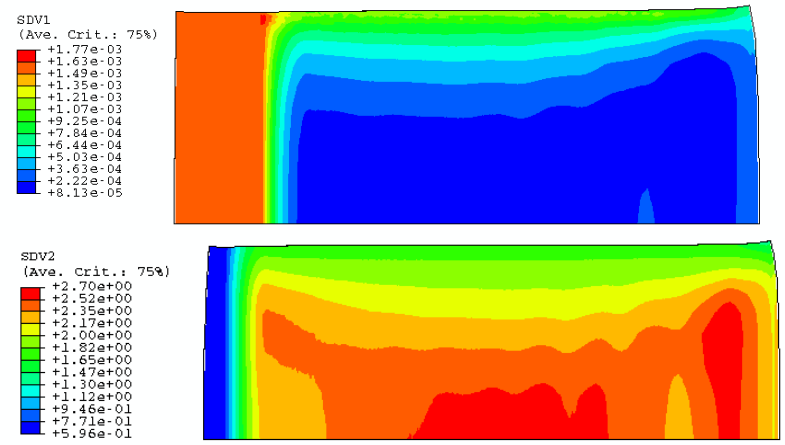

Figure 11. a) Porosity f during first pass. b) Void shape factor S at the end of the first pass.

In the second pass, edge cracks develop. This is illustrated in Figure 12. The picture also shows stress concentrations at the tips of the edge cracks, as one would expect. The fact that there are no cracks on the right side of the sheet is a consequence of a modeling detail: for computational reasons, the roll gap in the second pass is initially wider and closes gradually, when the sheet has already entered the roll gap. Only when the gap width approaches its final value, cracking starts to occur.

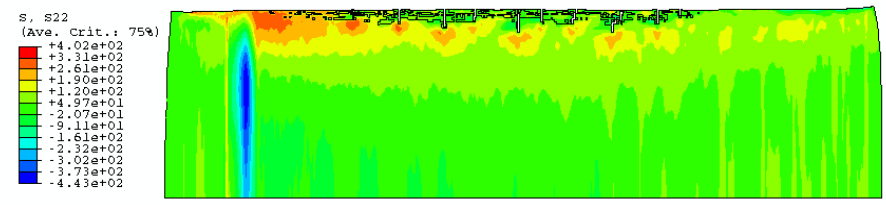

Figure 12. Stress in rolling direction during the second pass.

Figure 13 shows the porosity and the void shape factor in the second roll pass. Interestingly, it is not a single variable that assumes critical values in the cracked region, but it is the combination expressed by the Brown-Embury criterion, which becomes critical.

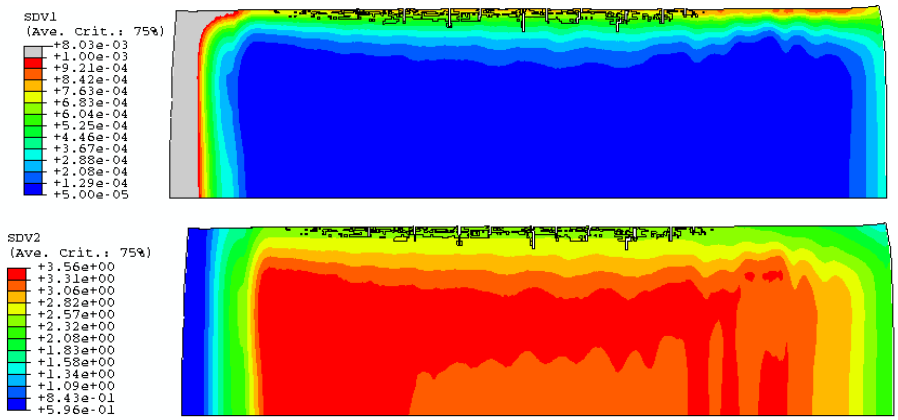

Figure 13. a) Porosity and b) void shape factor at the end of the second pass

The following two pictures show that the initial porosity f_0 has a great influence on edge cracking. Instead of the reference value $f_0 = 0.0016$ a slightly higher value $f_0 = 0.002$ is used here. Figure 14 shows that this moderate increase leads to enhanced edge cracking. Unfortunately, the value of f_0 cannot be determined accurately in the tensile test (see the Discussion). If the thickness reduction is increased in the first pass by 0.2 mm and reduced in the second by the same amount, cracking is further enhanced up to the point where the sheet ruptures entirely under the action of the coiling stress (Fig. 15).

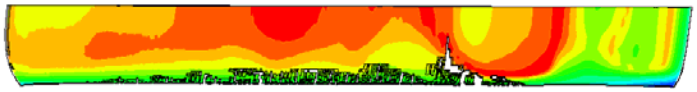

Figure 14. Enhanced edge cracking in the second pass for greater initial porosity, $f_0 = 0.002$. Colour plot for pore shape factor S

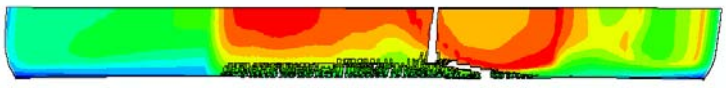

Figure 15. Greater thickness reduction in first pass, smaller reduction in second pass causes rupture during second pass. Initial porosity $f_0 = 0.002$.

Discussion

Experiments to determine the model parameters. In the present study, the tensile test was used to determine the model parameters. This is not ideal for the following reason: The tensile test activates void nucleation sites easily, whereas only few voids are nucleated during rolling (at least in the model), because the stress state is predominantly compressive, also near the edge of the sheet. In other words, failure of the tensile specimen is dominated by newly nucleated voids, whose volume fraction is represented by the model parameter f_N. Edge cracking, on the other hand, is dominated by the initial porosity f_0. This cannot be extracted from the tensile test, since it is overlaid by f_N, which is numerically much greater. Hence, a simple laboratory test needs to be developed, in which cracking occurs under higher hydrostatic pressure. First experiments with a special indentation test are promising. This test will allow measuring the model parameters including f_0 and assessing the sensitivity of a material against edge cracking.

Limitations of the Gologanu model. Although the Gologanu model is formulated on the continuum level for general three-dimensional stress states, it is derived from the analysis of axisymmetric voids. Therefore, it is questionable how accurate the predictions of the Gologanu model are for rolling, which leads to deformations that are different in all three directions. Therefore in the future, the simulations will be repeated with a model proposed by Ponte-Castaneda and co-workers [19,20], which considers ellipsoidal voids with three different axes. Other than the Gologanu model, the Ponte-Castaneda model also provides evolution equations for the orientation of the axes. Besides these advantages, the Ponte-Castaneda model has certain drawbacks, for example, relatively long computing times.

Multi-void models - Improvement of failure criteria. A means to explore the final instability of voided plastic materials are finite element models of specimens with many individually modeled voids. These investigations are in an initial stage, and the following preliminary results are shown only to illustrate the idea.

Figure 16a shows the finite element mesh around eight out of 204 voids in a plane-strain tensile specimen (from [15]). The initial porosity is 1%. The material between the voids is modeled by von Mises plasticity with power-law hardening (with hardening exponent $N = 0.03$ in this example). Figure 16b shows the whole specimen after plane strain tension. Apparently, failure occurs by strain localization. While the voids far away from the central area are still small and only slightly elongated, the voids in the center of the specimen have grown so large that they touch one another. At roughly 45°, slip bands with flat, elongated voids emanate from this central region. After final separation of the specimen halves, the fracture surface will exhibit a rough, dimpled central region and shear bands with relatively smooth surfaces towards the edges of the specimen.

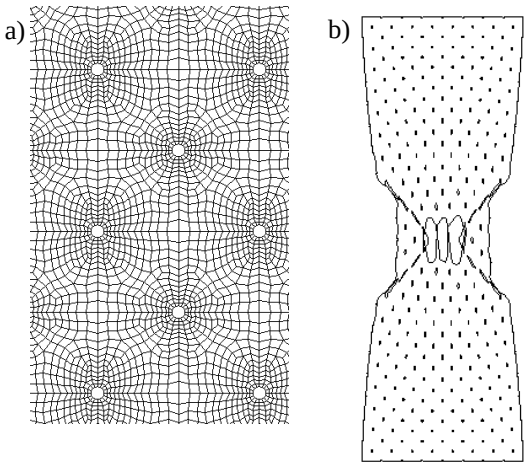

Figure 16. Localization in a multi-void model under plane strain tension. a) Cut-out of the model in the initial state, b) Strain localization in the center of the specimen and in shear bands

Figure 17shows a three-dimensional example with 255 individually modeled voids constituting an initial porosity 2.1%. Localization to the central plane happens at about 6% strain, and a load drop accompanies localization. Figure 17b shows the situation at about 10% strain.

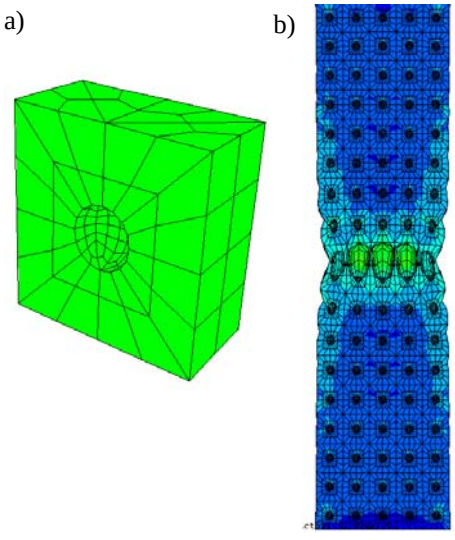

Figure 17. a) One out of 255 voids of a 3D model in the undeformed state, b) Localization at 10% strain.

In the future, such multi-void models can be used to calibrate the fracture criteria in combination with the Gologanu or similar damage mechanics models.

Summary and Conclusions

This paper presents a damage mechanics model that is able to describe edge cracking during rolling. The model predicts the characteristic zigzag pattern on the side surface of the sheet with angles that are very close to the observed ones. With this model, it is relatively easy to test process variants and to optimize the process on the computer, once the model parameters are known. For example, it was shown that an unfavorable distribution of a total thickness reduction to the individual rolling passes aggravates the problem of edge cracking. Depending on the thickness reduction in the previous and the present rolling passes and on the coiling stress, the edge cracks may lead to complete rupture of the sheet.

Model parameters were determined from tensile tests on an aluminum alloy. The test specimens had three different orientations, namely in the rolling, transverse and 45° directions. The data obtained from these tensile tests is not sufficient to determine all parameters unequivocally. The initial porosity remains uncertain, since the newly nucleated voids have a greater effect on crack formation in the tensile test. During rolling, on the other hand, only few new voids form, so that the growth and shape change of the initial voids determine the critical state for fracture. Therefore, a new type of test needs to be developed in which the stress history is closer to the situation prevailing at the edge of a sheet in the roll gap.

Acknowledgement. The authors from Fraunhofer IWM gratefully acknowledge financial support from the German National Science Foundation (DFG) under contract No. Ri 329/23.

References

[1] B. Dodd and P. Boddington: J. Mech. Working Technology 3 (1980) 239-252.
[2] P.F. Thomson and N.M. Burman: Mater. Sci. Eng. 45 (1980) 95-107.
[3] N.M. Burman and P.F. Thomson: J. Mech. Working Technology 13 (1986) 205-217.
[4] F. Andrieux, S. Oeser, J.G. Blauel, D.-Z. Sun and R. Böschen: Aluminium 77 (2001) 93-98 und 176-178.
[5] A.L. Gurson: J. Engng. Mater. Technology 99 (1977) 2-15.
[6] V. Tvergaard: Int. J. Fracture 17 (1981) 389-407.
[7] A. Needleman and V. Tvergaard: J. Mech. Phys. Solids 32 (1984) 461-490.
[8] H. Riedel: Fracture Mechanisms, in: Materials Science and Technology, R.-W. Cahn, P. Haasen and E.J. Kramer, Eds., Vol. 6: Plastic Deformation and Fracture of Materials, H. Mughrabi, Vol.-Ed., Chap. 12, VCH-Verlag, Weinheim, 1993, pp. 565-633.
[9] E. Parteder, H. Riedel and R. Kopp: Mater. Sci. Engng. A264 (1999) 17-25.
[10] M. Gologanu, J.B. Leblond and J. Devaux: J. Mech. Phys. Solids 41 (1993) 1723-1754.
[11] M. Gologanu, J.B. Leblond, G. Perrin, J. Devaux: CISM Courses and Lectures No. 377, ed. by P. Suquet (1997) 61-130.
[12] G.R. Johnson, W.H. Cook: Engg. Fracture Mech. 21 (1) (1985) 31-48.
[13] H. Hooputra, H. Gese, H. Dell, H. Werner: Int. J. Crash 9 (2004) 449-463.
[14] T. Wierzbicki, Y. Bao, Y.-W. Lee, Y. Bai: Int. J. Mech. Sci. 47 (2005) 719-743.
[15] H. Riedel, F. Andrieux, D-Z. Sun, T. Walde: Verbesserte konstitutive Modelle zur Beschreibung von Umformprozessen – Numerische Implementierung, Experimente und Anwendungen, Abschlussberichte zum DFG SPP 1074, R. Kopp, Hrsg., Deutsche Forschungsgemeinschaft, Bonn, 2005, S. 13-22.
[16] P.F. Thomason: Ductile Fracture of Metals, Oxford, Pergamon Press (1990).
[17] T. Pardoen, J.W. Hutchinson: J. Mech. Phys. Solids 48 (2000) 2467-2512.
[18] L.M. Brown, J.D. Embury: Proc. 3rd Int. Conf. on Strength of Metals and Alloys, Institute of Metals, London (1973).
[19] P. Ponte Castaneda, M. Kailasam: J. Mech. Phys. Solids 46 (1998) 427-465.
[20] M. Kailasam, N. Aravas, P. Ponte Castaneda: Computer Modeling in Engng. Sci. 1 (2000) 105-118.